Atmos. Chem. Phys., 7, 6075–6084, 2007
www.atmos-chem-phys.net/7/6075/2007/

Atmospheric Chemistry and Physics

Balloon-borne radiometer measurements of Northern Hemisphere mid-latitude stratospheric HNO_3 profiles spanning 12 years

M. Toohey[1], B. M. Quine[2], K. Strong[1], P. F. Bernath[3,4], C. D. Boone[4], A. I. Jonsson[1], C. T. McElroy[6], K. A. Walker[1,4], and D. Wunch[1,5]

[1]Department of Physics, University of Toronto, Toronto, ON, M5S 1A7, Canada
[2]School of Engineering, York University, Toronto, ON, M3J 1P3, Canada
[3]Department of Chemistry, University of York, Heslington, York, YO10 5DD, UK
[4]Department of Chemistry, Waterloo University, Waterloo, ON, N2L 3G1, Canada
[5]California Institute of Technology, Pasadena, CA, 91125, USA
[6]Environment Canada, Downsview, ON, M3H 5T4, Canada

Received: 2 July 2007 – Published in Atmos. Chem. Phys. Discuss.: 6 August 2007
Revised: 24 October 2007 – Accepted: 22 November 2007 – Published: 11 December 2007

Abstract. Low-resolution atmospheric thermal emission spectra collected by balloon-borne radiometers over the time span of 1990–2002 are used to retrieve vertical profiles of HNO_3, CFC-11 and CFC-12 volume mixing ratios between approximately 10 and 35 km altitude. All of the data analyzed have been collected from launches from a Northern Hemisphere mid-latitude site, during late summer, when stratospheric dynamic variability is at a minimum. The retrieval technique incorporates detailed forward modeling of the instrument and the radiative properties of the atmosphere, and obtains a best fit between modeled and measured spectra through a combination of onion-peeling and optimization steps. The retrieved HNO_3 profiles are consistent over the 12-year period, and are consistent with recent measurements by the Atmospheric Chemistry Experiment-Fourier transform spectrometer satellite instrument. We therefore find no evidence of long-term changes in the HNO_3 summer mid-latitude profile, although the uncertainty of our measurements precludes a conclusive trend analysis.

1 Introduction

One of the central aims of the Middle Atmosphere Nitrogen TRend Assessment (MANTRA) mission is to evaluate observational evidence for changes in the components of stratospheric total reactive nitrogen (NO_y) (Strong et al., 2005). Towards this aim, two emission radiometer instruments have played an important and unique role in the MANTRA balloon campaigns, due largely to the substantial flight heritage of the instrument design. The instruments measure atmospheric thermal emission in the 8–14 μm (715–1250 cm^{-1}) range, measuring the spectral emission features of many trace gas species, including emission at 11.3 μm due to nitric acid (HNO_3).

HNO_3 was first detected in the stratosphere by Murcray et al. (1968), who soon afterwards identified the 11.3-μm spectral band as ideal for the measurement of HNO_3 due to minimal interference by other gases (Murcray et al., 1973). Subsequent measurements, made primarily by balloon-borne filter radiometer instruments, led to a greater understanding of the vertical, latitudinal, and seasonal distribution of HNO_3 (Murcray et al., 1975) and the partitioning of active nitrogen between HNO_3, NO_2 and NO (e.g. Evans et al., 1977, 1982). Later measurements by many space-based instruments (see Santee et al., 2004, and references therein), and balloon-borne instruments such as MIPAS-B (Friedl-Vallon et al., 2004) and MkIV (Toon, 1991) have led to a wealth of retrieved HNO_3 profiles.

Unfortunately, deriving a picture of the long-term behaviour of HNO_3 using the historical archive of retrieved profiles is complicated by inconsistencies in the spectroscopic parameters used to retrieve profiles from radiance measurements. Laboratory measurements of the line intensities in the 11.3-μm band, in particular, have yielded results which differ by as much as 30% (Flaud et al., 2006). Retrieved volume mixing ratio (VMR) magnitudes have been seen to be directly proportional to scaling of the line intensities (e.g. Irion et al., 2002), thus it is fair to say that there exist systematic discrepancies between the various retrieved profiles, with magnitudes up to 30%.

Furthermore, modern computational resources have allowed the improvement of the algorithms used to retrieve

Correspondence to: M. Toohey
(mtoohey@atmosp.physics.utoronto.ca)

Published by Copernicus Publications on behalf of the European Geosciences Union.

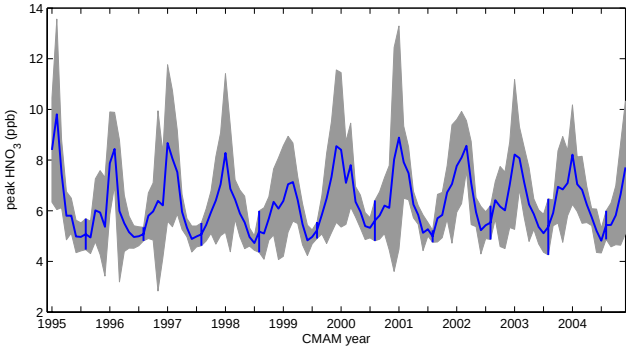

Fig. 1. Time series of monthly mean HNO_3 volume mixing ratio (VMR) at ∼24 km from the Canadian Middle Atmosphere Model (CMAM). Monthly variability (2σ) is represented by shading, and August variability values are highlighted by vertical lines.

trace gas profiles from radiance observations. The earliest retrievals were based upon an onion-peeling technique (e.g. Evans et al., 1976) which required smoothing of the raw data. Quine et al. (2005) have shown that the resulting profiles can be greatly affected by the somewhat arbitrary choice of smoothing parameters. Also, the ability of modern retrieval algorithms to perform global fits can greatly improve results (Irion et al., 2002).

In this work, we have collected data recorded by emission radiometer instruments during three MANTRA balloon flights (1998, 2000, and 2002), and during two flights in 1990. All data was collected through launches from a northern mid-latitude site (Vanscoy, Saskatchewan, 52° N, 107° W) during late summer when dynamical variability is minimal (Wunch et al., 2005). By analyzing the data with a consistent retrieval algorithm and spectroscopic line intensities, we connect modern measurements of HNO_3 with historical ones, and in so doing, develop a semi-quantitative picture of long-term HNO_3 profile changes.

2 HNO_3 in a changing atmosphere

HNO_3 is the principal component of NO_y in the lower stratosphere, where it acts as a reservoir for the active nitrogen species NO and NO_2 involved in catalytic ozone loss cycles.

Changes in the abundance of HNO_3 are related to changes in the abundance of NO_y and its partitioning. The source of stratospheric NO_y is the transport of N_2O from the troposphere. Tropospheric N_2O has steadily increased by 3% per decade due to anthropogenic activities. McLinden et al. (2001) estimate that this increase in N_2O should lead to a 2.3% per decade increase in NO_y, with the difference due to nonlinear NO_y loss processes in the upper atmosphere. Meanwhile, the partitioning of NO_y has been modified by the increase of stratospheric chlorine. Modelling studies by Prather et al. (1984) have shown that as stratospheric concentrations of inorganic chlorine increase, $ClONO_2$ becomes more important as a NO_y reservoir, leading to possible declines in HNO_3. HNO_3 is also highly sensitive to stratospheric aerosol loading through the heterogeneous reaction:

$$N_2O_5 + H_2O \rightarrow HNO_3 + HNO_3, \quad \text{(R1)}$$

which converts N_2O_5 to HNO_3 in the presence of aerosols.

Long-term changes in HNO_3 have been studied by use of ground-based observations of total columns, and space-based, vertically resolved HNO_3 profiles. In an analysis of data comprised of solar spectra recorded with a grating spectrometer in June 1951 and a set of observations obtained with a Fourier transform spectrometer between June 1986 and June 1990, all from the International Scientific Station of the Jungfraujoch in Swiss Alps, Rinsland et al. (1991) found no significant change in the June HNO_3 total column over this time span. Randel et al. (1999) report statistically significant decreases of order 2% per year in lower stratospheric, extra-tropical HNO_3 between 1993 and 1997 based on analysis of observations made by the Microwave Limb Sounder (MLS) on board the Upper Atmosphere Research Satellite (UARS). While the trend analysis excluded from consideration the MLS data from 1991–1992 in an attempt to remove the effects of elevated aerosol loading due to the Mt. Pinatubo eruption of 1991, ground-based measurements of HNO_3 total columns and model results indicate that NO_y partitioning may have been significantly perturbed until 1996 (Rinsland et al., 2003). To the authors' knowledge, no study has yet addressed long-term changes in HNO_3, apart from those due to aerosol loading from Mt. Pinatubo, by comparing consistent measurements from before and after the eruption.

The detection of trends in data is dependent upon the variability of the measured quantity (Weatherhead et al., 1998). In order to better understand the variability to be expected in HNO_3 profiles, we have studied simulated fields from the Canadian Middle Atmosphere Model. CMAM is an extended version of the Canadian Centre for Climate Modeling and Analysis spectral General Circulation Model. The dynamical core and chemistry scheme are described by Beagley et al. (1997) and de Grandpré et al. (1997) respectively. The current version of the model is discussed by Eyring et al. (2006), while the model results shown here are from a transient run described by Eyring et al. (2007). Chemical species have been saved every 18 h. Monthly mean CMAM HNO_3, at the vertical level of peak VMR (∼24 km) and the model gridpoint closest to Vanscoy, Saskatchewan, are shown in Fig. 1 for ten years of the transient run. The seasonal cycle is apparent in the model output, with maximum HNO_3 in winter, and minimum in summer. The 2σ monthly variability of the 18-hourly data is shown by the shaded region. The average standard deviation of August HNO_3 values is approximately 6% of the mean, while in winter the same metric is 16%. Summer measurements are therefore the most useful measurements for assessing long-term changes in HNO_3.

3 Instrument design and history

The emission radiometer instruments used in this study were originally designed and fabricated by the Canadian Atmospheric Environment Service (AES) in the early 1970's and used on balloon campaigns until the 1980's (e.g. Evans et al., 1977, 1982). The instruments were produced based on a design first developed by Pick and Houghton (1969) and later used to measure HNO_3 by Murcray et al. (1973). The main design features include (see Quine et al., 2005, Fig. 2): a mechanical chopper at the entrance slit, a spectral band-pass filter, a mercury-cadmium-telluride detector, amplifying electronics, and an insulated liquid-nitrogen dewar surrounding the detector and optics, maintaining a temperature of approximately 77 K. The instrument design also includes a blackbody calibration flap that is automatically lowered to cover the field-of-view periodically. The flap, mounted externally to maintain a temperature above that of liquid nitrogen, has an embedded platinum resistance thermometer to provide temperature information necessary for performing in-flight radiometric calibration.

The radiometer measures the cumulative spectroscopic gas emission along an upward-looking slant path. Vertical atmospheric information is made available by mounting the instrument, typically with a 20° elevation angle, on a balloon platform, and taking measurements while the balloon ascends. At the beginning of the balloon ascent, the instrument views a slant path through the whole atmosphere, and the radiance measurements are at a maximum. As the instrument ascends, the atmosphere below the instrument is excluded from the slant path, and the collected radiance decreases. A radiosonde is flown with the instrument in order to measure temperature and pressure, from which altitude is deduced via the hydrostatic relation.

When first fabricated, these instruments were furnished with five discrete band-pass filters to sample sections of the HNO_3 emission band at 11.3 μm. Radiance estimates were derived from these band-pass measurements and a careful filter calibration. Later instrument designs replaced the discrete filters with circular variable filter (CVF) segments. With two segments mounted on a constantly turning wheel, the instruments are able to scan a wavelength region from 8–14 μm (715–1250 cm^{-1}) with a band-pass varying between 1% and 4% of the center wavelength. A number of these scanning emission radiometers were flown on a series of AES test flights from Vanscoy, Saskatchewan from 1989–1991 before being used in non-recovered Arctic flights. Two surviving instruments, code-named MX-31 and MX-36 were refurbished with minimal modifications and used in the biennial MANTRA flights of 1998–2004.

4 Retrieval

Vertical profiles of HNO_3 were originally retrieved from data measured by the emission radiometer instrument through an onion-peeling algorithm, wherein the amount of HNO_3 between two measurement altitudes was assumed to be proportional to the change in radiance between the measurements (Evans et al., 1976). Instrument parameters were determined through pre- and post-flight calibration.

Quine et al. (2005) introduced a new retrieval algorithm for the emission radiometer, based on detailed forward modelling of the atmosphere and instrument. Given atmospheric temperature and pressure information, expected trace gas abundances, and some instrument calibration parameters, these models simulate the spectral scans recorded by the instrument during flight. An optimization routine is used to obtain a best fit between the simulated and measured spectra by adjusting the instrument parameters and trace gas amounts. The main advantage of this technique is the incorporation of instrument parameters into the retrieved state vector, which allows the analysis of flight data without pre- and post- calibration data. We summarize the main points of the retrieval algorithm below, with special emphasis on modifications made since the work of Quine et al. (2005).

4.1 Atmospheric forward model

The atmosphere is modelled as a set of discrete 2-km-thick cells on a vertical grid. For each cell, a density-weighted effective mean temperature and pressure are determined using the Curtis-Godson approximation (Houghton, 1986), based on sonde measurements. Spectral absorption coefficients for each cell and for eight principal emitting gas species (H_2O, CO_2, O_3, N_2O, CH_4, HNO_3, CFC-11 and CFC-12) are calculated using the GENSPECT line-by-line code (Quine and Drummond, 2002) with HITRAN 2004 data (Rothman et al., 2005). HITRAN line parameter updates for HNO_3 are included (Flaud et al., 2006), based on work that went into the MIPAS (Michelson Interferometer for Passive Atmospheric Sounding) database. Radiative transfer code included in the GENSPECT package is used to calculate the radiance at each cell boundary based on the blackbody emission and transmission of each cell. This simulated spectral radiance profile is linearly interpolated to the radiometer measurement heights, and passed as the main input into the instrument forward model.

4.2 Instrument forward model

The aim of the instrument forward model is to accurately simulate the true mapping between input radiance and detector response. While it is assumed that the individual instruments are for the most part functionally identical, a few instrument parameters defining unique properties of the instruments are necessary, and are included in the forward model.

Two parameters define the mapping between CVF angular position and wavenumber. A linear relationship between CVF position and wavelength is reported by the CVF manufacturer and assumed here. Initial estimates for the two parameters are produced manually by finding the angular position of the O_3 and HNO_3 peaks in the raw data. These instrument parameters are then included in the retrieval, and serve to shift and stretch the wavenumber axis of the measured spectra in order to match the simulated spectra.

A third instrument parameter is used in the construction of the instruments' slit function. The shape of the slit function, and the relationship between width and center wavelength is based upon Fourier transform spectrometer measurements of the bandpass of a sample CVF. A retrieved instrument parameter specifies the width of a boxcar function convolved with this experimental slit function, accounting for the finite angular width of the focussed light passing through the CVF in each particular instrument.

While mercury-cadmium-telluride detectors are known to exhibit non-linear response to radiation (e.g. Borrello et al., 1977; Abrams et al., 1994), laboratory tests have shown the emission radiometer instruments to respond nearly linearly to blackbody radiation over much of their measurement range. Assuming such an idealized linear relationship, the instrument is modelled such that detector response S at a given wavenumber ν', altitude z, and incident radiance spectrum I for a given effective viewing angle $\hat{\theta}$ be given by:

$$S(\nu', z) = R(\nu', z) \int_0^\infty I(\nu, \hat{\theta}, z) F(\nu - \nu') d\nu + \epsilon, \qquad (1)$$

where R is the instrument responsivity, F is the slit function, and ε is a dark current level.

Dark current noise is defined for each scan by the average signal measured as an opaque section of the CVF attenuates the input radiation.

The effective viewing angle $\hat{\theta}$ is an approximate quantity describing the mean elevation angle of light collected by the instrument. It is a function of the mounting angle of the instrument on the balloon payload, the field-of-view (FOV) function of the instrument describing the angular dependence of the instrument's ability to collect radiation, and the radiation field as a function of angle. In order to define a constant $\hat{\theta}$ for any measurement set, we assume a plane parallel atmosphere with homogeneous emission. The radiation field is then given by the cosecant function describing the variation of atmospheric slant path with elevation angle, and $\hat{\theta}$ is given by the mean of the product of the FOV and cosecant functions. The FOV, as determined by laboratory tests, is roughly toroidal, with sensitivity extending to $\pm 16°$ and maximum sensitivity at $\pm 9°$. The effective viewing angle for an instrument mounted at 20° elevation angle is approximately 17°.

In-flight blackbody calibration scans, performed every fifth scan at altitudes z', are used to define instrument responsivity function R. The responsivity of the instrument changes as a function of altitude, most likely due to the fact that the detector does not typically reach liquid nitrogen temperature before launch, and continues to cool during the balloon ascent. The responsivity function is calculated as the ratio of detector output S (with dark current ϵ subtracted) to the theoretical blackbody radiance curve (based on the temperature measured by the flap thermometer, assuming the flap has a blackbody emissivity of unity) convolved with the instrument slit function:

$$R(\nu', z') = \frac{S(\nu', z') - \epsilon}{\int_0^\infty B_\nu(\nu, T) F(\nu - \nu') d\nu}. \qquad (2)$$

The responsivity function is then interpolated to the atmospheric measurement heights (z) in order to calculate the simulated spectra via Eq. (1).

4.3 Optimization

The objective function is defined as the sum of squares of the difference between the simulated and measured spectral scans. The optimal retrieval is that which minimizes this objective function.

The spectral range of the optimization is restricted to 825–945 cm^{-1}, a spectral window which includes strong emission features from HNO_3 as well as from the interfering species CFC-11 and CFC-12. Since there is significant overlap of the spectral features from these three species in the spectral window used due to the low resolution of the instruments, all three species are necessarily retrieved. The remaining species included in the atmospheric forward model are represented by constant a priori profiles.

Prior work (Quine et al., 2005) introduced the use of a non-linear optimization algorithm used to search for a global minimum of the objective function by iteratively perturbing the full state vector of instrument parameters and trace gas species on the full vertical grid. While this technique produced reasonable results, it required large amounts of computing resources, and time. In order to produce results on a faster time scale we have modified this approach.

In the current approach, the optimization routine is used to retrieve a reduced state vector composed of instrument parameters and scale factors which multiply trace gas profiles. This reduces the state space of the optimization from the order of 30 (3 species by 10 altitudes) to six (3 scale factors + 3 instrument parameters). We use the Direct routine (Jones et al., 1993) to perform the optimization, although any global search algorithm could be employed.

The optimization routine is used in tandem with an onion-peeling routine which modifies the altitude structure of the profiles while keeping the instrument parameters fixed. Starting at the uppermost atmospheric cell and moving down, trace gas amounts are adjusted in order to minimize the measurement residual within that cell in the local spectral neighbourhood of the emission peak for each of the three species. The onion-peeling proceeds by the method of steepest descent, with the local gradient defined by first perturbing the

cell VMR by 1%, and using the forward model to calculate the corresponding change in radiance. This process is repeated iteratively until the difference between the measured and simulated radiances reaches a preset convergence criterion. Weighting functions and averaging kernels for the onion-peeling algorithm are given in Quine et al. (2005), wherein it was used as a first-pass retrieval only.

The profile-scaling and onion-peeling steps are iterated alternatively as described above with one exception: the objective function to be minimized for the first optimization step is based solely on spectral scans within the lowermost atmospheric cell since at low altitudes, all three retrieved species show significant spectral features. The presence of three emission "peaks" allows the proper estimation of both the wavenumber-calibration-stretching and bandpass-filter-width instrument parameters. At higher altitudes, where only HNO_3 emission is significant, the effects of these two instrument parameters are indistinguishable. Experience has shown that this first-pass optimization is generally successful in identifying the correct "valley" of the full objective function state space, which can have a great number of local minima.

Comparison of simulated and measured spectral scans for a sample instrument and year are shown in Fig. 2.

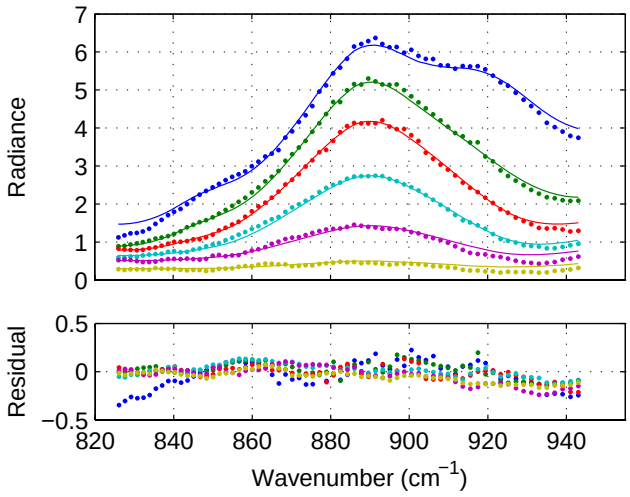

Fig. 2. An example selection of spectral fits and residuals, approximately equally spaced between 12 and 30 km height, from the emission radiometer fitting routine. Results shown are for MANTRA 2000, MX-36. Plotted points represent the measurement scans, while lines show the simulated spectra.

4.4 Error analysis

Within the final onion peeling step of the retrieval, a root-mean-square (RMS) residual is calculated between the simulated and measured spectra in the neighbourhood of the emission peak for each gas species fit. This RMS value acts as a measure of the radiance noise. In order to estimate the retrieval error based on this noise, a Jacobian matrix describing the forward modeled change in radiance for a given change in species mixing ratio is created through a sensitivity study. Retrieval errors are then calculated based on the inverse of this Jacobian matrix, and we are therefore able to estimate the error in each retrieved species based on the radiance noise present in the spectral peaks of all three species.

The recorded temperature of the blackbody flaps is another major source of uncertainty. Laboratory tests have produced calibration coefficients for the two instruments used in MANTRA flights. Based on these tests, we conservatively estimate the thermometer measurement error of the MANTRA blackbody flaps as 2 K. Corresponding VMR errors have been calculated by simply performing the retrieval on raw data perturbed by the temperature uncertainty estimate. A 2 K error in temperature leads to a HNO_3 VMR error of approximately 10% at 24 km.

The uncertainty in the effective elevation angle is estimated to be $\pm 0.5°$, which corresponds to an error of approximately 2.5% at 24 km.

Radiance error, blackbody temperature error, and viewing angle error are added in quadrature to obtain the total retrieval error as a function of altitude.

Finally, the retrieval altitudes themselves have errors as a result of uncertainty in the measurement of pressure by the sonde, and the propagation of this uncertainty through the hydrostatic equation. Assuming an uncertainty of 1 hPa, we estimate the corresponding error in altitude from Fig. 4 of Richner and Viatte (1995). Altitude error is on the order of a few meters below 20 km, but grows exponentially with height and reaches ± 2 km at 35 km.

This error analysis does not take into account errors due to the assumption of linear detector response. Blackbody tests have shown that while the response of the instrument is nearly linear over its full measurement range, non-linear response is apparent at the lowest measured radiances. Correction of non-linear effects would require characterization of the detectors used in each instrument. Since the retrieval method used here aims to be useful for historical flights for which the instruments are no longer available, we maintain our assumption of linearity. The effect of non-linear detector response would likely be systematic biases, especially at higher altitudes where measured radiances are at a minimum.

5 Data

Each MANTRA mission has included on the instrument payload two radiometers, MX-31 and MX-36. The two instruments were mounted with different elevation angles, with one at 20° and the other at 30–40°. Raw data of good quality was collected by both instruments during the flights of 1998 and 2000. One instrument failed in 2002, and both

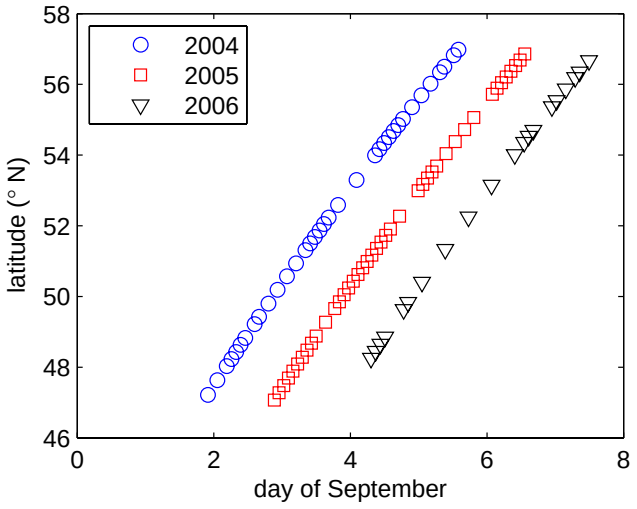

Fig. 3. Time-latitude coordinates of Northern Hemisphere mid-latitude ACE occultations in late summer, over three years.

instruments failed in 2004, likely due to the effect of ice build-up on the mechanically rotating CVF.

The AES test flights of 1990 suffered from a variety of fatal and non-fatal failures, making the raw data difficult to process. All flights suffered from poor data quality due to transponder drop-outs. Many flights also suffered from obvious miscalibration of the blackbody flap temperatures.

We include in this work results from two radiometer flights of August 1990. Of all data from the AES test flights, that from MX-19 on August 30 is of the highest quality. The ubiquitous transponder drop-outs and a higher-than-expected spectral noise are the data's only significant faults. Data from MX-13, flown on 20 August 1990, suffered some more critical non-fatal effects. Time synchronization between the radiometer clock and the radiosonde clock (in order to achieve proper altitude registration) was produced by defining a time offset that minimized the residual between the time derivatives of the sonde-measured air temperature and the instrument flap temperature. Furthermore, the flap temperature was bias corrected in order to bring the difference between flap temperature and air temperature into a range comparable to the other flights. Due to these necessary pre-processing steps, we have estimated the temperature error of the blackbody flaps for this flight at 5 K.

We will compare our retrieved profiles of HNO_3, CFC-11 and CFC-12 with results from the Atmospheric Chemistry Experiment – Fourier transform spectrometer (hereinafter ACE) satellite instrument, launched in August 2003. We compare with ACE since it simultaneously retrieves all three species measured by the radiometers, and since ACE data has previously been used in a trend analysis of many species, including CFC-11 and CFC-12 (Rinsland et al., 2005). ACE is a Fourier transform spectrometer operating at high spectral resolution in the infrared, measuring atmospheric extinction by solar occultation, from which profiles of temperature, pressure and dozens of constituents are retrieved through a global fitting algorithm (Bernath et al., 2005; Boone et al., 2005). ACE results are from the version 2.2 data set. HNO_3 retrievals from ACE employ a set of microwindows near 900 cm^{-1} (11.3 μm), and another set near 1700 cm^{-1}, and use the HITRAN 2004 spectral database. ACE retrievals do not use the Flaud et al. (2006) HNO_3 update, but the impact of the update to HITRAN 2004 in the 11.3-μm spectral range is small: the percent change in integrated line intensity over this band is on the order of 2% (Flaud et al., 2006). ACE retrievals have been shown to have good (relative differences of 5–10% below 30 km) agreement with MIPAS operational retrievals (Wang et al., 2007a), and the MIPAS IMK-IAA research product (Wang et al., 2007b). Due to the orbit and solar occultation technique used by the ACE platform, the latitudinal distribution of measurements is highly dependent upon the time of year. ACE samples the Northern mid-latitudes in late summer briefly at the beginning of September (see Fig. 3), in close proximity to the window of past MANTRA flights (24 August–3 September). For the comparison, we take the average of a total of 97 late summer ACE measurements from 2004–2006 over the 10° latitude band centered on the latitude of Vanscoy, Saskatchewan.

Table 1. Balloon flights of the radiometer dataset.

Flight	Date	Instruments
AES	20 August 1990	MX13
AES	30 August 1990	MX19
MANTRA	24 August 1998	MX31, MX36
MANTRA	29 August 2000	MX31, MX36
MANTRA	3 September 2002	MX31

6 Results

The retrieved profiles of HNO_3 are shown in Fig. 4. An overall MANTRA-mean HNO_3 profile is calculated based on the weighted mean profiles for 1998 and 2000, and the single measured profile in 2002, and is shown on each panel for comparison. The retrieved profiles are quite consistent. The two retrieved profiles for the flights with simultaneous measurements (1998 and 2000) are equivalent at almost all altitudes. Differences between the simultaneous measurements may be due to differences in horizontal sampling by the two instruments mounted with differing elevation angles, and the local horizontal gradient in the HNO_3 field, or due to different non-linear response of the instrument detectors as discussed in Sect. 4.4. The error in the 1990 profiles is large, due to uncertainties in the blackbody flap temperature and

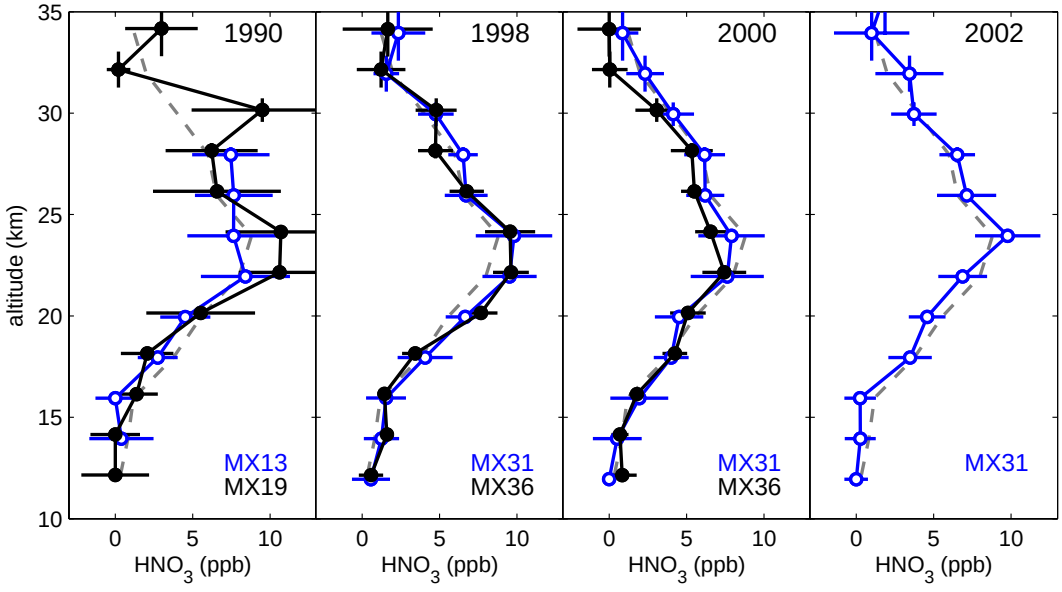

Fig. 4. Retrieved HNO_3 profiles for the years shown. Instrument code names, specifying the source of the radiance data used in each retrieval, are given in the legend (see Table 1). Horizontal error bars show the estimated total uncertainty in the retrievals, vertical error bars show the estimated error in altitude. The mean profile over MANTRA missions (1998–2002) is shown by the dashed line.

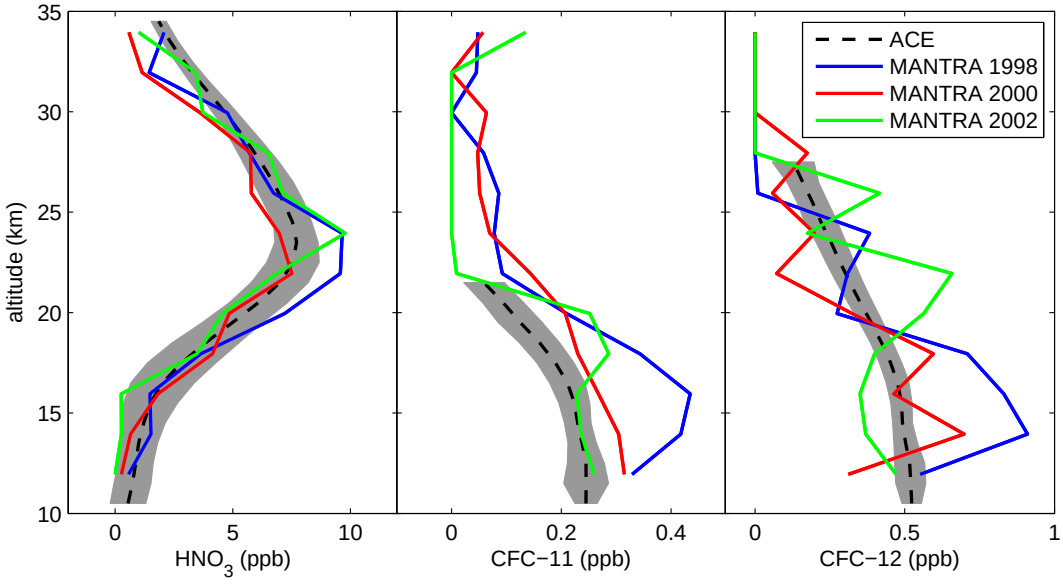

Fig. 5. Profiles of HNO_3, CFC-11 and CFC-12 VMR from the MANTRA flights and from observations by the ACE satellite instrument (2004–2006). Shading represents the 2σ variability of the ACE profile.

the measured radiance noise. Despite this, the profiles are not inconsistent with the MANTRA mean profile.

MANTRA yearly mean profiles of HNO_3, CFC-11 and CFC-12 are compared to mean Northern Hemisphere mid-latitude late summer retrieved profiles from the ACE satellite instrument in Fig. 5. The comparison shows good agreement for HNO_3: the MANTRA HNO_3 profiles lie within the ACE 2σ variability for most altitudes. The retrieved HNO_3 is slightly larger than the ACE profiles at the peak values around 24 km for MANTRA 1998 and 2002. Also, the MANTRA profiles are low compared to ACE at high altitudes: this may be due to the non-linear response of the

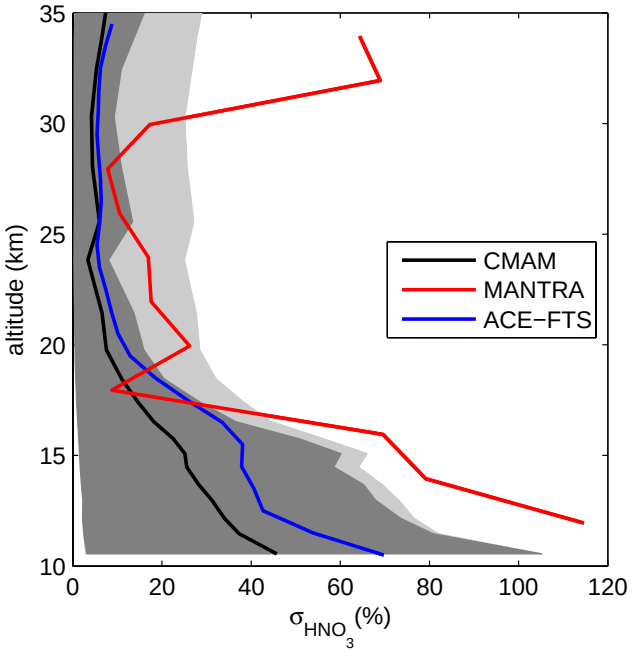

Fig. 6. Percent standard deviations of HNO_3 VMR profiles from ACE measurements, MANTRA measurements, and simulated fields from CMAM. Grey shading represents the 99% confidence interval of values given by CMAM when only three independent samples are used (dark grey), and with an added 10% error on each sample (light grey).

detectors at low radiance levels, or due to altitude errors. The CFC profiles retrieved from the radiometer measurements as interfering species exhibit a large degree of scatter. Compared to ACE, the retrieved CFC-11 profiles are biased high, especially for the MANTRA 1998 flight. CFC-12 shows no obvious bias, but shows significant oscillations with height. The weaker emission of the CFCs leads to a more difficult retrieval: the estimated errors for the individual CFC profiles (not shown) range from approximately 20% at low altitudes to greater than 100% at high altitudes where the mixing ratios are small. Given the difficulty of the CFC retrieval, we argue that retrieving values within a factor of two of the ACE mean profiles is acceptable.

Are the MANTRA HNO_3 measurements consistent with the variability of the CMAM? Figure 6 addresses this question by plotting the percent standard deviation of the three yearly mean MANTRA profiles and that from the 18-hourly model data from the final week of August over 10 CMAM years. The two profiles show similar structure, with larger values in the lower stratosphere, and a broad minimum between 20 and 30 km. This comparison is somewhat unfair as the MANTRA HNO_3 measurements represent a very sparse sampling of the true HNO_3 late-summer time series, with only three independent samples. We address the issue of sparse sampling by MANTRA by calculating the standard deviation of the model profiles using only three random samples. By iterating this procedure a large number of times, we produce a probability distribution function of the calculated standard deviation for the given MANTRA sampling, and define a 99% confidence interval, shown in dark grey shading in Fig. 6. By repeating the same procedure, but adding a 10% random error onto the sampled CMAM profiles, we get an even better sense of the variability expected in the MANTRA measurements (light grey). Between 18 and 30 km height, the variability of the MANTRA measurements is seen to be consistent with the variability of the model, given the sparsity and uncertainty of the measurements. Above 30 km and below 18 km, the variance of the MANTRA measurements is apparently adversely affected by instrument error.

The variance of ACE HNO_3 measurements is in excellent agreement with that of the CMAM (Fig. 6). On the one hand, this close agreement validates our use of the model to explore the sampling issues inherent in the MANTRA measurements. On the other hand, under the assumption that the CMAM gives a good estimate of the variability of the true atmosphere, any difference between the CMAM and ACE variances should be due to the random error of the ACE retrievals. The close agreement between the measured and modelled variance is then evidence that ACE measurements display a high degree of precision, which is consistent with the small errors estimated for ACE (typically 1–5% for HNO_3 between 10 and 35 km) based on analysis of random spectroscopic fitting errors (Boone et al., 2005).

7 Conclusions

We have analyzed raw data recorded by low-resolution scanning infrared radiometers from balloon flights in 1990, 1998, 2000, and 2002, and retrieved vertical profiles of HNO_3 using current spectroscopic line parameters and an efficient retrieval technique making use of both optimization and onion-peeling retrieval routines. The measurements were taken over a mid-latitude Northern Hemisphere site in late summer, when stratospheric dynamical and chemical variability is minimal. The retrieved HNO_3 profiles show good agreement, in profile shape and magnitude, with measurements made by the ACE satellite instrument at a similar season and latitude region over the years 2004–2006. The variance of the HNO_3 profiles measured over the MANTRA era (1998–2002) is in good agreement with the variability estimated by the CMAM, when the limited sampling and error of the measurements are taken into account. The radiometer measurements represent a consistent data set with samples before and after the Mt. Pinatubo eruption of 1991 which perturbed NO_y partitioning, and hence HNO_3 levels, through the injection of aerosols into the stratosphere. The UARS MLS instrument, which began observation soon after the Mt. Pinatubo eruption, found a significant trend in HNO_3 over the time span 1993–1997 (Randel et al., 1999) after aerosol levels had

decreased to near background levels. Modelling results suggest that this measured trend may have been due to a slow relaxation to pre-Mt. Pinatubo eruption conditions, rather than any underlying long-term trend (Rinsland et al., 2003). We have compared retrieved HNO_3 profiles from before and well after the Mt. Pinatubo eruption and found no significant difference, however, the uncertainty of our measurements precludes conclusive confirmation of the slow relaxation hypothesis.

Acknowledgements. All four MANTRA campaigns were supported by the Canadian Space Agency (CSA) and the Meteorological Service of Canada. MANTRA 1998 also received support from the Centre for Research in Earth and Space Technology, while MANTRA 2002 and 2004 were also supported by Natural Sciences and Engineering Research Council (NSERC) of Canada. The Atmospheric Chemistry Experiment (ACE), also known as SCISAT-1, is a Canadian-led mission mainly supported by the CSA and NSERC. This work was also carried out with the aid of a grant from the CSA. M. Toohey gratefully acknowledges the scholarship support of NSERC and the CSA.

Edited by: A. Richter

References

Abrams, M., Toon, G., and Schindler, R.: Practical example of the correction of Fourier-transform spectra for detector nonlinearity, Appl. Optics, 33, 6307–6314, 1994.

Beagley, S. R., de Grandpré, J., Koshyk, J. N., McFarlane, N. A., and Shepherd, T. G.: Radiative-dynamical climatology of the first-generation Canadian Middle Atmosphere Model, Atmos. Ocean, 35, 293–331, 1997.

Bernath, P. F., McElroy, C. T., Abrams, M. C., Boone, C. D., Butler, M., Camy-Peyret, C., Carleer, M., Clerbaux, C., Coheur, P.-F., Colin, R., DeCola, P., DeMazière, M., Drummond, J. R., Dufour, D., Evans, W. F. J., Fast, H., Fussen, D., Gilbert, K., Jennings, D. E., Llewellyn, E. J., Lowe, R. P., Mahieu, E., McConnell, J. C., McHugh, M., McLeod, S. D., Michaud, R., Midwinter, C., Nassar, R., Nichitiu, F., Nowlan, C., Rinsland, C. P., Rochon, Y. J., Rowlands, N., Semeniuk, K., Simon, P., Skelton, R., Sloan, J. J., Soucy, M.-A., Strong, K., Tremblay, P., Turnbull, D., Walker, K. A., Walkty, I., Wardle, D. A., Wehrle, V., Zander, R., and Zou, J.: Atmospheric Chemistry Experiment (ACE): Mission overview, Geophys. Res. Lett., 32, L15S01, doi:10.1029/2005GL022386, 2005.

Boone, C. D., Nassar, R., Walker, K. A., Rochon, Y., McLeod, S. D., Rinsland, C. P., and Bernath, P. F.: Retrievals for the atmospheric chemistry experiment Fourier-transform spectrometer, Appl. Optics, 44, 7218–7231, 2005.

Borrello, S., Kinch, M., and LaMont, D.: Photoconductive HgCdTe Detector Performance With Background Variations, Infrared Phys., 17, 121–125, 1977.

de Grandpré, J., Sandilands, J. W., Mcconnell, J. C., Beagley, S. R., Croteau, P. C., and Danilin, M. Y.: Canadian Middle Atmosphere Model: Preliminary results from the chemical transport module, Atmos. Ocean, 35, 385–431, 1997.

Evans, W. F. J., Lin, C. I., and Midwinter, C. L.: The Altitude Distribution of Nitric Acid at Churchill, Atmosphere, 14, 172–179, 1976.

Evans, W. F. J., Kerr, J. B., McElroy, C. T., Obrien, R. S., Wardle, D. I., and Ridley, B. A.: The odd nitrogen mixing ratio in the stratosphere, Geophys. Res. Lett., 4, 235–238, 1977.

Evans, W. F. J., Kerr, J. V., McElroy, C. T., O'Brien, R. S., and McConnell, J. C.: Measurements of NO_2 and HNO_3 during a stratospheric warming at 54 in February 1979, Geophys. Res. Lett., 9, 493–496, 1982.

Eyring, V., Waugh, D. W., Bodeker, G. E., Cordero, E., Akiyoshi, H., Austin, J., Beagley, S. R., Boville, B., Braesicke, P., Brühl, C., Butchart, N., Chipperfield, M. P., Dameris, M., Deckert, R., Deushi, M., Frith, S. M., Garcia, R. R., Gettelman, A., Giorgetta, M., Kinnison, D. E., Mancini, E., Manzini, E., Marsh, D. R., Matthes, S., Nagashima, T., Newman, P. A., Nielsen, J. E., Pawson, S., Pitari, G., Plummer, D. A., Rozanov, E., Schraner, M., Scinocca, J. F., Semeniuk, K., Shepherd, T. G., Shibata, K., Steil, B., Stolarski, R., Tian, W., and Yoshiki, M.: Multi-model projections of stratospheric ozone in the 21st century, J. Geophys. Res., 112, doi:10.1029/2006JD008332, 2007.

Eyring, V., Butchart, N., Waugh, D. W., Akiyoshi, H., Austin, J., Bekki, S., Bodeker, G. E., Boville, B. A., Brühl, C., Chipperfield, M. P., et al.: Assessment of temperature, trace species, and ozone in chemistry-climate model simulations of the recent past, J. Geophys. Res., 111, doi:10.1029/2006JD007327, 2006.

Flaud, J.-M., Brizzi, G., Carlotti, M., Perrin, A., and Ridolfi, M.: MIPAS database: Validation of HNO_3 line parameters using MIPAS satellite measurements, Atmos. Chem. Phys., 6, 5037–5048, 2006, http://www.atmos-chem-phys.net/6/5037/2006/.

Friedl-Vallon, F., Maucher, G., Seefeldner, M., Trieschmann, O., Kleinert, A., Lengel, A., Keim, C., Oelhaf, H., and Fischer, H.: Design and Characterization of the Balloon-Borne Michelson Interferometer for Passive Atmospheric Sounding (MIPAS-B2), Appl. Optics, 43, 3335–3355, 2004.

Houghton, J. T.: The Physics of Atmospheres, Cambridge University Press, 1986.

Irion, F. W., Gunson, M. R., Toon, G. C., Chang, A. Y., Eldering, A., Mahieu, E., Manney, G. L., Michelsen, H. A., Moyer, E. J., Newchurch, M. J., et al.: Atmospheric Trace Molecule Spectroscopy (ATMOS) Experiment Version 3 data retrievals, Appl. Optics, 41, 6968–6979, 2002.

Jones, D. R., Perttunen, C. D., and Stuckman, B. E.: Lipschitzian optimization without the Lipschitz constant, J. Optimiz. Theory App., 79, 157–181, 1993.

McLinden, C. A., Olsen, S. C., Prather, M. J., and Liley, J. B.: Understanding trends in stratospheric NO_y and NO_2, J. Geophys. Res., 106, 27 787–27 793, 2001.

Murcray, D. G., Kyle, T. G., Murcray, F. H., and Williams, W. J.: Nitric acid and nitric oxide in the lower stratosphere, Nature, 218, 78–79, 1968.

Murcray, D. G., Goldman, A., Csoeke-poeckh, A., Murcray, F. H., Williams, W. J., and Stocker, R. N.: Nitric acid distribution in the stratosphere, J. Geophys. Res., 78, 7033–7038, 1973.

Murcray, D. G., Barker, D. B., Brooks, J. N., Goldman, A., and Williams, W. J.: Seasonal and latitudinal variation of the stratospheric concentration of HNO_3, Geophys. Res. Lett., 2, 223–225, 1975.

Pick, D. R. and Houghton, J. T.: Measurements of atmospheric infrared emission with a balloon-borne multifilter radiometer, Q. J. Roy. Meteor. Soc., 95, 535–543, 1969.

Prather, M. J., McElroy, M. B., and Wofsy, S. C.: Reductions in ozone at high concentrations of stratospheric halogens, Nature, 312, 227–231, 1984.

Quine, B. M. and Drummond, J. R.: GENSPECT: A new generation line-by-line code with a bounded interpolation accuracy, J. Quant. Spectrosc. Ra., 74, 147–165, 2002.

Quine, B. M., Toohey, M., Drummond, J. R., Strong, K., Wunch, D., Midwinter, C., and McElroy, C. T.: The Concentration Profile of Nitric Acid and Other Species over Saskatchewan in August 1998: Retrieval from Data Recorded by Thermal-Emission Radiometry, Atmos. Ocean, 43, 361–376, 2005.

Randel, W. J., Wu, F., Russel III, J. M., and Waters, J.: Space-time patterns of trends in stratospheric constituents derived from UARS measurements, J. Geophys. Res., 104, 3711–3728, 1999.

Richner, H. and Viatte, P.: The Hydrostatic Equation in the Evaluation Algorithm for Radiosonde Data, J. Atmos. Ocean. Tech., 12, 649–656, 1995.

Rinsland, C. P., Zander, R., and Demoulin, P.: Ground-based infrared measurements of HNO_3 total column abundances: long-term trend and variability, J. Geophys. Res., 96, 9379–9389, 1991.

Rinsland, C. P., Weisenstein, D. K., Ko, M. K. W., Scott, C. J., Chiou, L. S., Mahieu, E., Zander, R., and Demoulin, P.: Post-Mount Pinatubo eruption ground-based infrared stratospheric cloumn measurements of HNO_3, NO and NO_2 and their comparison with model calculations, J. Geophys. Res., 108, 4437, doi:10.1029/2002JD002965, 2003.

Rinsland, C. P., Boone, C., Nassar, R., Walker, K., Bernath, P., Mahieu, E., Zander, R., McConnell, J. C., and Chiou, L.: Trends of HF, HCl, CCl_2 F_2, CCl_3F, $CHClF_2$ (HCFC-22), and SF_6 in the lower stratosphere from Atmospheric Chemistry Experiment (ACE) and Atmospheric Trace Molecule Spectroscopy (ATMOS) measurements near 30° N latitude, Geophys. Res. Lett., 32, doi:10.1029/2005GL022415, 2005.

Rothman, L. S., Jacquemart, D., Barbe, A., Chris Benner, D., Birk, M., Brown, L. R., Carleer, M. R., Chackerian, C., Chance, K., Coudert, L. H., et al.: The HITRAN 2004 molecular spectroscopic database, J. Quant. Spectrosc. Ra., 96, 139–204, 2005.

Santee, M. L., Manney, G. L., Livesey, N. J., and Read, W. G.: Three-dimensional structure and evolution of stratospheric HNO_3 based on UARS Microwave Limb Sounder measurements, J. Geophys. Res., 109, doi:10.1029/2004JD004578, 2004.

Strong, K., Bailak, G., Barton, D., Bassford, M. R., Blatherwick, R. D., Brown, S., Chartrand, D., Davies, J., Drummond, J. R., Fogal, P. F., et al.: Mantra-A Balloon Mission to Study the Odd-Nitrogen Budget of the Stratosphere, Atmos. Ocean, 43, 283–299, 2005.

Toon, G.: The JPL MkIV interferometer, Opt. Photonics News, 2, 19–21, 1991.

Wang, D. Y., Höpfner, M., Blom, C. E., Ward, W. E., Fischer, H., Blumenstock, T., Hase, F., Keim, C., Liu, G. Y., Mikuteit, S., Oelhaf, H., Wetzel, G., Cortesi, U., Mencaraglia, F., Bianchini, G., Redaelli, G., Pirre, M., Catoire, V., Huret, N., Vigouroux, C., Mazière, M. D., Mahieu, E., Demoulin, P., Wood, S., Smale, D., Jones, N., Nakajima, H., Sugita, T., Urban, J., Murtagh, D., Boone, C. D., Bernath, P. F., Walker, K. A., Kuttippurath, J., Kleinböhl, A., Toon, G., and Piccolo, C.: Validation of MIPAS HNO_3 operational data, Atmos. Chem. Phys., 7, 4905–4934, 2007a.

Wang, D. Y., Höpfner, M., Tsidu, G. M., Stiller, G. P., von Clarmann, T., Fischer, H., Blumenstock, T., Glatthor, N., Grabowski, U., Hase, F., et al.: Validation of nitric acid retrieved by the IMK-IAA processor from MIPAS/ENVISAT measurements, Atmos. Chem. Phys., 7, 721–738, 2007b.

Weatherhead, E. C., Reinsel, G. C., Cheang, W. K., Tiao, G. C., Meng, X. L., Choi, D., Keller, T., DeLuisi, J., Wuebbles, D. J., and Kerr, J. B.: Factors affecting the detection of trends- Statistical considerations and applications to environmental data, J. Geophys. Res., 103, 17–149, 1998.

Wunch, D., Tingley, M. P., Shepherd, T. G., Drummond, J. R., Moore, G. W. K., and Strong, K.: Climatology and predictability of the late summer stratospheric zonal wind turnaround over Vanscoy, Saskatchewan, Atmos. Ocean, 43, 301–313, 2005.